Neurobiology of Disease 127 (2019) 362–373

Contents lists available at ScienceDirect

Neurobiology of Disease

journal homepage: www.elsevier.com/locate/ynbdi

Upregulation of tripeptidyl-peptidase 1 by 3-hydroxy-(2,2)-dimethyl butyrate, a brain endogenous ligand of PPARα: Implications for late-infantile Batten disease therapy

Sudipta Chakrabarti[a,1], Sujyoti Chandra[a,1], Avik Roy[a,b], Sridevi Dasarathi[a], Madhuchhanda Kundu[a], Kalipada Pahan[a,b,*]

[a] Department of Neurological Sciences, Rush University Medical Center, Chicago, USA
[b] Division of Research and Development, Jesse Brown Veterans Affairs Medical Center, Chicago, USA

ARTICLE INFO

Keywords:
3-Hydroxy-(2,2)-dimethyl butyrate
TPP1
LINCL
PPARα

ABSTRACT

The late-infantile Batten disease or late-infantile neuronal ceroid lipofuscinosis (LINCL) is an autosomal recessive lysosomal storage disorder caused by mutations in the *Cln2* gene leading to deficiency of lysosomal enzyme tripeptidyl peptidase 1 (TPP1). At present, available options for this fatal disorder are enzyme replacement therapy and gene therapy, which are extensively invasive and expensive. Our study demonstrates that 3-hydroxy-(2,2)-dimethyl butyrate (HDMB), a brain endogenous molecule, is capable of stimulating TPP1 expression and activity in mouse primary astrocytes and a neuronal cell line. HDMB activated peroxisome proliferator-activated receptor-α (PPARα), which, by forming heterodimer with Retinoid X receptor-α (RXRα), transcriptionally upregulated the *Cln2* gene. Moreover, by using primary astrocytes from wild type, PPARα$^{-/-}$ and PPARβ$^{-/-}$ mice, we demonstrated that HDMB specifically required PPARα for inducing TPP1 expression. Finally, oral administration of HDMB to Cln2 heterozygous (*Cln2*$^{+/-}$) mice led to a marked upregulation of TPP1 expression in the motor cortex and striatum in a PPARα-dependent fashion. Our study suggests that HDMB, a brain endogenous ligand of PPARα, might have therapeutic importance for LINCL treatment.

1. Introduction

The Neuronal ceroid lipofuscinosis (NCL) comprises a group of clinically related hereditary lysosomal storage diseases that primarily occurs during childhood. They exhibit severe neurodegenerative conditions and collectively represent the most predominant neurodegenerative disorders in children with age of onset ranging from birth through early adulthood (Nita et al., 2016; Schulz et al., 2013). These fatal disorders are clinically characterized by progressive cognitive decline, mental deterioration, impairment of motor function, retinopathy leading to loss of vision and seizures (Nita et al., 2016; Sleat et al., 1999; Hachiya et al., 2006; Warrier et al., 2013). In spite of having diverse biochemical etiology, a spectrum of symptoms and disease severity, all forms of NCLs share common histopathological features marked by excessive accumulation of autofluorescent ceroid lipopigments in neurons and other cells (Nita et al., 2016; Warrier et al., 2013). Classically NCLs were grouped based on age of onset, type of storage material; however recently, NCLs have been classified into 14 categories (CLN1-14) based on genetic origin (Williams and Mole, 2012; Mole and Cotman, 2015).

The classic late-infantile NCL (LINCL), formerly known as Jansk'y-Bielschowsky disease (OMIM #204500), is caused by mutations in the CLN2 gene resulting in deficiency in the activity of the lysosomal enzyme tripeptidyl peptidase 1 (TPP1) (EC 3.4.14.9) (Sleat et al., 1997). The Cln2 gene (Ceroid lipofuscinosis, neuronal, 2) (MIM #607998) is a 6.65 kb gene comprised of 13 exons and 12 introns mapped to chromosome 11p15.5. (Liu et al., 1998; Haines et al., 1998) and encodes a 563-amino acid containing TPP1 preproenzyme which following removal of signal peptide, glycosylation and cleavage yields the 367 residue long 46 kD mature active TPP1 enzyme (Golabek et al., 2003; Sondhi et al., 2001). The protein TPP1 progressively eliminates tripeptides from the N-terminus of small polypeptides, one of which is the

Abbreviations: LINCL, late-infantile neuronal ceroid lipofuscinosis; Cln2, Ceroid lipofuscinosis, neuronal 2; TPP1, Tripeptidyl peptidase 1; HDMB, 3-Hydroxy-(2,2)-dimethyl butyrate; PPARα, peroxisome proliferator-activated receptor α

* Corresponding author at: Department of Neurological Sciences, Rush University Medical Center, 1735 West Harrison St, Suite Cohn 310, Chicago, IL 60612, USA.
E-mail address: Kalipada_Pahan@rush.edu (K. Pahan).

[1] First two authors have equal contribution to the work.

https://doi.org/10.1016/j.nbd.2019.03.025
Received 7 January 2019; Received in revised form 11 March 2019; Accepted 24 March 2019
Available online 28 March 2019
0969-9961/

subunit c of mitochondrial ATP synthase (SCMAS), the major constituent of the storage granules in LINCL (Crystal et al., 2004; Sohar et al., 1999). Classical LINCL manifests at 2 to 4 years of age followed by the disease course involving seizures, ataxia, myoclonus, developmental delay, speech impairment, progressive neuronal death leading to deterioration of locomotor functions and vision making the patients reach a vegetative state and ultimately death by 8 to 12 years of age (Sondhi et al., 2001; Worgall et al., 2008; Xu et al., 2011; Haltia, 2003). At the ultrastructural level, curvilinear autofluorescent ceroid-lipofuscin granules accumulate in the lysosomes of neurons causing extensive neuronal death by apoptosis (Sondhi et al., 2001; Worgall et al., 2008; Lane et al., 1996).

Gene therapy, enzyme-replacement therapy and stem cell transplantation have been widely explored in animal models as well as human patients for treatment of LINCL. Recently, enzyme replacement therapy using intraventricular infusion of cerliponase alfa (recombinant human TPP1) in children with CLN2 disease has demonstrated reduced impairment of locomotor and language functions; however the mode of treatment was fairly invasive and was associated with a battery of adverse side effects (Schulz et al., 2018). Therefore, at present, there is a requirement for novel, less invasive treatment options for LINCL. Studies have suggested that residual TPP1 activity is retained in LINCL patients, suggesting that a limited number of functional copies of the Cln2 gene are present in these patients (Sleat et al., 1999; Viglio et al., 2001; Walus et al., 2010). Therefore, drug-mediated therapeutic strategies targeted towards augmenting the expression and residual activity of TPP1 could be of potential benefit for LINCL treatment.

Our lab has demonstrated that FDA-approved fibrate drugs Gemfibrozil and Fenofibrate upregulate TPP1 in brain cells via activation of peroxisome proliferator-activated receptor α (PPARα) (Ghosh et al., 2012). Interestingly, our recent study identified a novel endogenous ligand of PPARα, 3-hydroxy-(2,2)-dimethyl butyrate (HDMB), from mouse hippocampus and described a role for HDMB in inducing synaptic functions (Roy et al., 2016). Given the previous evidence that HDMB activates PPARα, we examined whether HDMB could stimulate TPP1 in mouse brain cells and in a CLN2 mouse model. Here, we demonstrate that HDMB upregulated TPP1 expression in MN9D neuronal cells as well as mouse primary astrocytes via PPARα. Furthermore, oral administration of HDMB enhanced TPP1 levels in the motor cortex and striatum of *Cln2*$^{+/-}$, but not *Cln2*$^{+/-}$*PPARα*$^{-/-}$, mice. Finally, we delineate the underlying mechanism that HDMB stimulates PPARα to form a transcriptional complex on the *Cln2* gene promoter to upregulate the expression of *Cln2*. Therefore, upregulation of TPP1 by a brain endogenous molecule, HDMB, might have therapeutic implications for LINCL.

2. Materials and methods

2.1. Reagents

DMEM 1×, DMEM F-12 50/50 1×, Hanks' balanced salt solution (HBSS 1×), and 0.05% trypsin were obtained from Mediatech (Washington, D. C.). Fetal bovine serum (FBS) was purchased from Atlas Biologicals (Fort Collins, CO). Neurobasal media and B27 supplement were purchased from Invitrogen (San Diego, CA). Antibiotic-antimycotic and other cell culture reagents were obtained from Sigma. 3-hydroxy-(2,2)-dimethyl butyrate (HDMB) was obtained from Santacruz Biotechnology Inc. For details on antibodies, please see Table 1.

2.2. Animals

Animal maintaining and experiments were in accordance with National Institute of Health guidelines and were approved by the Institutional Animal Care and Use committee (IACUC) of the Rush University of Medical Center, Chicago, IL. Animals exhibiting mild seizures and tremors were fed and watered through animal feeding needles. However, if any mouse came to the moribund stage, it was decapitated after anesthesia with ketamine/xylazine injectables. Conditions for moribund were as follows: Central nervous system disturbance (Head tilt, Seizures, Tremors, Circling, Spasticity, and Paresis); Inability to remain upright; Evidence of muscle atrophy; Chronic diarrhea or constipation; Rough coat and distended abdomen; Spreading area of alopecia caused by disease; Coughing, rales, wheezing and nasal discharge; Distinct jaundice and/or paleness (anemia); Markedly discolored urine, polyuria or anuria; Frank bleeding from any orifice; Persistent self-induced trauma.

Cln2$^{(+/-)}$ animals were kindly provided by Dr. Peter Lobel (Center for Advanced Biotechnology and Medicine, Robert Wood Johnson Medical School, Piscataway, New Jersey, USA). These animals were inbred and subsequent generations were screened by RT-PCR to further obtain *Cln2*$^{+/+}$ *and Cln2*$^{+/-}$ strains.

2.3. Treatment of *Cln2*$^{+/-}$ mice with HDMB

Age- and sex-matched *Cln2*$^{+/+}$ mice from the same background were used as wild type (WT) controls and *Cln2*$^{+/-}$ animals were used in different treatment groups. HDMB (5 mg/kg body wt/day) was dissolved in 0.1% methyl cellulose (MeC). *Cln2*$^{+/-}$ mice were either not fed (control group), gavaged with 0.1% MeC (vehicle-treated group) or gavaged with HDMB (HDMB-treated group) for 2 weeks for biochemical studies.

2.4. Cells

MN9D neuronal cell line was obtained from Dr. A. Heller (University of Chicago, Chicago, IL, USA) and maintained in the lab. Cells were grown in Dulbecco's modified Eagle's medium (Thermo Fisher Scientific, Waltham, MA) supplemented with 10% (*v*/v) heat-inactivated fetal bovine serum and allowed to differentiate in neurobasal media containing 2% B27, glutamine and 1% antibiotic–antimycotic solution (Sigma). For experiments, prior to HDMB treatment, cells were incubated in neurobasal media containing B27 minus antioxidants.

2.5. Isolation of mouse primary astroglia

Mouse primary astroglia were isolated from mixed glial cultures as previously described (Brahmachari and Pahan, 2007; Saha and Pahan, 2007) and following the procedure of Giulian and Baker (Giulian and Baker, 1986). Mixed glial cultures isolated from pups were maintained in Dulbecco's modified Eagle's medium/F-12-50/50. On day 9, the cultures are subjected to shaking at 240 rpm for 2 h at 37 °C on a rotary shaker for the elimination of microglia. On day 11, the shaking was performed for 24 h for the elimination of oligodendroglia. This ensures the complete elimination of all non-astroglial cells from the culture. The attached cells were astroglia. For experiments, cells were seeded onto new plates and grown for 1 to 2 days before treatment.

2.6. Semi-quantitative reverse transcriptase-coupled PCR (RT-PCR)

Total RNA was isolated from mouse primary astrocytes and MN9D neuronal cells using the Qiagen RNA-Easy kit (Valencia, CA) following the manufacturer's protocol. Semi-quantitative reverse-transcriptase PCR was performed according to standard procedure (Khasnavis et al., n.d.; Khasnavis and Pahan, n.d.). Isolated RNA was converted to cDNA using oligo(dT)$_{12–18}$ as primer and MMLV RT (Moloney murine leukemia virus reverse transcriptase) (Invitrogen) in a 20-μl reaction mixture. The cDNA was appropriately amplified by PCR reactions using Promega Master Mix (Madison, WI) and the following primers (Invitrogen) for murine genes: mouse *Cln1*, sense 5′-ACACAGAGGACCGC CTGGGG-3′ and antisense 5′-TCATGCACGGCCCACACAGC-3′; mouse

Table 1
Antibodies, sources, applications, and dilutions used in this paper.

Target	Antibody (clone)	Epitope/Immunogen	Application/Dilution	Source; Catalog
β-Actin	Mouse monoclonal (AC-15)	a.a. 1–15 of *Xenopus laevis* β-actin	WB – 1:5000	Abcam; ab6276
TPP1	Rabbit monoclonal EPR16537	aa 350–500 Recombinant fragment within Human TPP1.	WB – 1:5000 IF – 1:1000	Abcam; ab195234
GFAP	Rabbit polyclonal	Synth peptide to cow GFAP	IHC – 1:2000	Dako; z0334
TH	Rabbit polyclonal	SDS denatured from rat TH	IF – 1:1500	PelFreez Biologicals; P40101-150
PPARα	Mouse monoclonal (3B6)	Recombinant full-length protein	ChIP – 1:200	Abcam; ab2779
PPARβ	Mouse monoclonal (F-10) X TransCruz antibody	Amino acids 2–75 of PPARβ of mouse origin	ChIP – 1:50	Santa cruz Biotechnology Inc., sc-74,517
PPARγ	Rabbit monoclonal (81B8)	Synthetic peptide corresponding to residues surrounding His494 of human PPARγ	ChIP – 1:100	Cell signaling Technology, 2443S
PGC1α	Mouse monoclonal (4C1.3)	Recombinant protein consisting of amino acids 1–120 of mouse PGC-1α	ChIP – 1:1000	EMD Millipore, ST1202
RXRα	Rabbit monoclonal (D6H10)	Synthetic peptide corresponding to residues near the amino terminus of human RXRα protein	ChIP – 1:100	Cell Signaling Technology Inc., 3085

TPP1, tripeptidyl peptidase I; TH, tyrosine hydroxylase; GFAP, glial fibrillary acidic protein; PPAR, peroxisome proliferator-activated receptor; RXR, retinoid X receptor; PGC1α, PPARγ coactivator 1 alpha; WB, Western blot; IF, immunofluorescence; ChIP, chromatin immunoprecipitation.

Cln2, sense 5′-CACCATCCAGTTACTTCAATGC-3′ and antisense 5′-CTG ACCCTCCACTTCTTCATTC-3′; mouse *Cln3*, sense 5′-TGCTGCCCTGCC ATCGAGTG-3′ and antisense 5′-GGCAGCGCTCAGCATCACCA-3′; and mouse *GAPDH*, sense 5′- GCACAGTCAAGGCCGAGAAT-3′ and antisense 5′-GCCTTCTCCATGGTGGTGAA-3′. Amplified PCR products were electrophoresed on 2% agarose (Invitrogen) gels and detected by ethidium bromide (Invitrogen). The expression of *Glyceraldehyde-3-phosphate dehydrogenase* (*GAPDH*) was used as a loading control.

2.7. Quantitative real-time PCR

As described before (Ghosh et al., 2012), quantitative real-time PCR was performed using the ABI-Prism7700 sequence detection system (Applied Biosystems, Foster City, CA) using SYBR green. The mRNA expression of the target gene was normalized to the expression of *GAPDH* mRNA. The fold change in expression of the treated with respect to the untreated control was calculated and represented.

2.8. Immunostaining of cells

Immunocytochemistry was performed as described before (Khasnavis et al., n.d.; Khasnavis and Pahan, n.d.). Briefly, MN9D cells or primary astrocytes were seeded onto square cover glass in 6-well plates and cultured to 70–80% confluency. Following treatment, cells were fixed using chilled methanol (Fisher) overnight, followed by two brief wash with filtered PBS. Cells were blocked using 2% BSA (Fisher) in PBSTT (PBS containing Tween 20 (Sigma) and Triton X-100 (Sigma)) for 30 min and further incubated with primary antibody (in PBS) at room temperature under gentle shaking conditions for 2 h [primary antibodies: TPP1 (1:200; Santa Cruz Biotechnology); *GFAP* (1:100; Santa Cruz Biotechnology)]. Next, cells were washed with filtered PBS (15 min washes, 4times) and incubated with Cy2- or Cy5-labeled secondary antibodies (1:200; Jackson ImmunoResearch) for 1 h under gentle shaking conditions. Following wash in PBS (15 min washes, 4times), cells were further incubated with 4′,6-diamidino-2-phenylindole (DAPI, 1:10,000; Sigma) for 4 to 5 min. The cover glass was mounted on glass slides, ran through ethanol and xylene (Fisher) gradient and visualized under Olympus BX41 fluorescence microscope.

2.9. Immunostaining of tissue sections

It was performed as described previously (Ghosh et al., 2012; Dasgupta et al., 2004). After 14 days of HDMB treatment, mice were perfused using PBS. Hemibrains were incubated in 4% paraformaldehyde followed by 30% sucrose and embedded. Free floating sections were made from different brain regions. For immunohistochemistry, following blocking in 2% BSA, sections were incubated with *TPP1* (1:200) and *NeuN* (1:100) primary antibodies. The sections were mounted, ran through ethanol and xylene gradient and observed under Olympus BX41 fluorescence microscope.

2.10. Immunoblotting

Western blotting was conducted as described in earlier studies (Ghosh et al., 2012; Corbett et al., n.d.; Saha et al., 2006) with minor modifications. Briefly, cells were scraped in PBS and lysed in RIPA buffer. Proteins were electrophoresed on 12% SDS/PAGE gels and transferred onto nitrocellulose membrane (Bio-Rad) using the Thermo-Pierce Fast Semi-Dry Blotter. Next, the membrane was blocked for 1 h using Li-Cor Odyssey blocking solution (Li-COR, Lincoln, NE) and incubated overnight with primary antibody at 4 °C under shaking conditions [primary antibodies: *TPP1* (1:250, Abcam) and *β-actin* (1:800; Abcam)] (Table 1). The following day, membranes were washed in PBST four times (15 min each) and incubated in secondary antibodies against the primary antibody hosts (all 1:10,000; Li-COR) for 1 h at room temperature. Next, the membrane is washed for 1 h with PBST and visualized under the Odyssey Infrared Imaging System (Li-COR, Lincoln, NE).

2.11. TPP1 activity assay

It was performed as described by Vines and Warburton (Vines and Warburton, 1999) with modifications (Ghosh et al., 2012). Briefly, cells were homogenized and 20 μg protein was mixed with substrate (40 μl) in individual wells of a polystyrene 96-well plate (Nalge Nunc International). The substrate solution consisted of 250 μmol/l Ala-Ala-Phe 7-amido-4-methylcoumarin (catalog no. A3401; Sigma; diluted freshly from a 25 mmol/l stock dissolved in dimethyl sulfoxide and stored at −20 °C) in substrate dilution buffer (0.15 mol/l NaCl, 1 g/l Triton X-100, 0.1 mol/l sodium acetate, adjusted to pH 4.0). Following addition, the plate was briefly centrifuged to remove bubbles and placed in 37 °C. Before taking the reading, the plate was mixed for 10 s. The plate was read in Victor X2 microplate reader (Perkin Elmer) from the bottom using 360/20 nm excitation and 460/25 nm emission filters. Optimum substrate and protein concentrations were determined using different concentrations prior to the assay.

2.12. Chromatin immunoprecipitation (ChIP) assay

It was performed using the method described by Nelson et al. (Nelson et al., 2006), with modifications (Ghosh et al., 2012). Briefly, MN9D cells were stimulated by 10 μM and 20 μM HDMB for 2 h followed

by fixing with formaldehyde (1.42% final volume) and quenching with 125 mM glycine. Next, the cells were pelleted and lysed in IP buffer (150 mM NaCl, 50 mM Tris-HCl (pH 7.5), 5 mM EDTA, Nonidet P-40 (0.5% v/v), Triton X-100 (1.0% v/v). For 500 ml, add 4.383 g of NaCl, 25 ml of 100 mM EDTA (pH 8.0), 25 ml of 1 M Tris-HCl (pH 7.5), 25 ml of 10% (v/v) Nonidet P-40, and 50 ml of 10% (v/v) Triton X-100 containing the following inhibitors: 10 μg/ml leupeptin, 0.5 mM phenylmethylsulfonyl fluoride (PMSF), 30 mM *p*-nitrophenyl phosphate, 10 mM NaF, 0.1 mM Na_3VO_4, 0.1 mM Na_2MoO_4, and 10 mM β-glycerophosphate) (Ghosh et al., 2012). Following a wash with 1.0 ml IP buffer, the pellet was resuspended in 1 ml IP buffer (containing all inhibitors), and sonicated. The sheared chromatin was divided into two fractions (one for using as Input). The remaining fraction was incubated with 5 μg of primary antibodies (anti-PPARα, anti-PPARβ, anti-PPARγ, and anti-PGC1α) and normal IgG overnight under rotation at 4 °C followed by incubation with protein G-agarose (Santa Cruz Biotechnology) for 2 h at 4 °C under rotating conditions. Next, beads were washed five times with cold IP buffer, and 100 μl of 10% Chelex (10 g/100 ml H_2O) was added directly to the beads and vortexed. Following 10 min boiling, the Chelex/protein G bead suspension was allowed to cool to room temperature. Proteinase K (100 μg/ml) was added, and the beads were incubated for 30 min at 55 °C while shaking, followed by another round of boiling for 10 min. Next, the suspension was centrifuged, and the supernatant was collected. The Chelex/protein G beads fraction was vortexed with another 100 μl of water, centrifuged again, and the first and the second supernatants were combined. The eluate was used directly as a template for PCR. The following primers were used for PCR reactions to amplify fragments flanking the *RXR*-binding element on the mouse *Cln2* promoter: Set1, sense 5′-CAG CTG CCA TGT CCC CCA GC-3′ and antisense 5′-TGC GCA GCT CTG TGT CAT CCG-3′; Set2, sense 5′-GCT CCC TCT CCT CAG CTG CCA-3′ and antisense 5′-CAT CCG GAG GCT CCA GGC CA-3′ (Ghosh et al., n.d.-a). The PCR reaction was standardized by using varying cycle numbers and different amounts of templates so that the results were in the linear range of PCR (Ghosh et al., n.d.-a; Ghosh et al., n.d.-b).

2.13. Densitometric analysis

Immunoblots blots were analyzed using ImageJ (National Institutes of Health, Bethesda) and bands were normalized with their respective β-actin loading controls. Data represents the average fold change with respect to untreated control for three independent experiments.

2.14. Statistics

Statistical analyses were performed with Student's *t*-test (for two-group comparisons) and one-way ANOVA, followed by Tukey's multiple-comparison tests, as appropriate (for multiple groups comparison), using Prism 7 (GraphPad Software). Data represented as mean ± SD or mean ± SEM as stated in figure legends. A level of $p < .05$ was considered statistically significant.

3. Results

3.1. HDMB upregulates TPP1 expression in MN9D neuronal cells

We first examined whether HDMB could upregulate TPP1 levels in MN9D cells, a mouse neuronal cell line. In this regard, we analyzed the mRNA expression of different *Cln* genes, *Cln1*, *Cln2* and *Cln3*, which, when mutated, cause infantile, late infantile and juvenile forms of NCL respectively. Semi-quantitative RT-PCR data showed that HDMB, at 20 μM dose, remarkably upregulated the expression of *Cln1*, *Cln2* and *Cln3* mRNA in a time-dependent manner (Fig. 1A). This was further confirmed by a similar pattern of increase in the expression of these genes in real-time PCR (Fig. 1B). Since HDMB showed the highest effect at 4 h time point, we conducted a dose-dependent study with 4 h treatment of different doses (10, 20 and 30 μM) of HDMB in MN9D cells. Interestingly, semi-quantitative and real-time PCR data showed that HDMB was able to increase *Cln1*, *Cln2* and *Cln3* mRNA expression at 10 and 20 μM concentrations; however the effect decreased at 30 μM HDMB (Fig. 1C, D). Next, we checked the protein expression of TPP1, the lysosomal enzyme encoded by the *Cln2* gene. Parallel to our previous results, HDMB was able to upregulate the protein levels of TPP1 in a dose-dependent manner in MN9D cells (Fig. 1E, F). Similarly, immunocytochemistry revealed a marked increase in TPP1 expression in TH-positive MN9D cells following 20 μM HDMB treatment (Fig. 1G). Finally, we evaluated whether HDMB-mediated upregulation of TPP1 mRNA and protein also results in enhanced functionality of this protease. We performed an enzymatic assay for TPP1 in MN9D cells and observed a profound increase in the activity of TPP1 with 20 μM HDMB treatment (Fig. 1H). Taken together, these results indicate that HDMB augments the expression and activity of TPP1 in MN9D neuronal cells.

3.2. HDMB enhances TPP1 expression in mouse primary astrocytes

Next, we checked the effect of HDMB on TPP1 expression in wild type (WT) mouse primary astrocytes. Similar to our findings in MN9D neuronal cells, we observed that in primary astrocytes, HDMB distinctly increased the mRNA expression of *Cln1*, *Cln2* and *Cln3* in a dose-dependent fashion as demonstrated by semi-quantitative RT-PCR and real-time PCR (Fig. 2A, B). We further analyzed the expression of TPP1 with different doses of HDMB treatment and observed that HDMB was able to significantly upregulate TPP1 protein levels with 20 μM showing the highest increase (Fig. 2C, D). This was further validated by immunocytochemistry which revealed marked upregulation with 20 μM HDMB treatment (Fig. 2E). Next, we analyzed the activity of the TPP1 enzyme following HDMB treatment. Consistent with our earlier observation in MN9D cells, data showed that 20 μM HDMB was able to significantly augment the activity of TPP1 in primary astrocytes. Collectively, these data suggest that HDMB increases TPP1 levels and activity in mouse primary astrocytes.

3.3. HDMB requires PPARα for increasing TPP1 expression

After establishing the role of HDMB in upregulation of TPP1, we intended to delineate the upstream mechanisms. In a previous study, we had established that PPARα agonist gemfibrozil increases TPP1 expression in brain cells via forming heterodimer with retinoid X receptor-α (Ghosh et al., 2012). Indeed, PPARs are known to form transcriptional complex with RXR and regulate the expression of target genes (Heneka and Landreth, 2007). Based on the previous evidence that HDMB is an endogenous ligand of PPARα (Roy et al., 2016) and PPARα agonist enhances TPP1 expression (Ghosh et al., 2012), we speculated that HDMB might activate PPARα to upregulate TPP1. To explore this, we transduced MN9D neuronal cells with lentivirus containing a dominant-negative construct of PPARα, Y464D (Fig. 3A), or with lentivirus containing GFP which served as a control. The Tyrosine 464 residue is a key site for binding of HDMB to PPARα ligand-binding domain and the dominant-negative construct Y464D inhibits the binding (Roy et al., 2016). Following transduction, we analyzed the expression of different *Cln* genes by semi-quantitative and real-time PCR. As expected, HDMB significantly upregulated the mRNA expression of *Cln1*, *Cln2* and *Cln3* in the *Lenti-GFP*-transduced cells; however, the effect of HDMB was abrogated in the *Lenti-Y464D-PPARα*-transduced MN9D cells (Fig. 3B, C), indicating that HDMB is not able to increase the expression of these genes in the absence of PPARα. Immunoblot analysis also revealed similar pattern of results where HDMB-mediated upregulation of TPP1 expression was drastically abolished in the presence of *Lenti-Y464D-PPARα* construct (Fig. 3D, E). Together, these results demonstrate that HDMB requires PPARα for increasing TPP1 expression in MN9D neuronal cells.

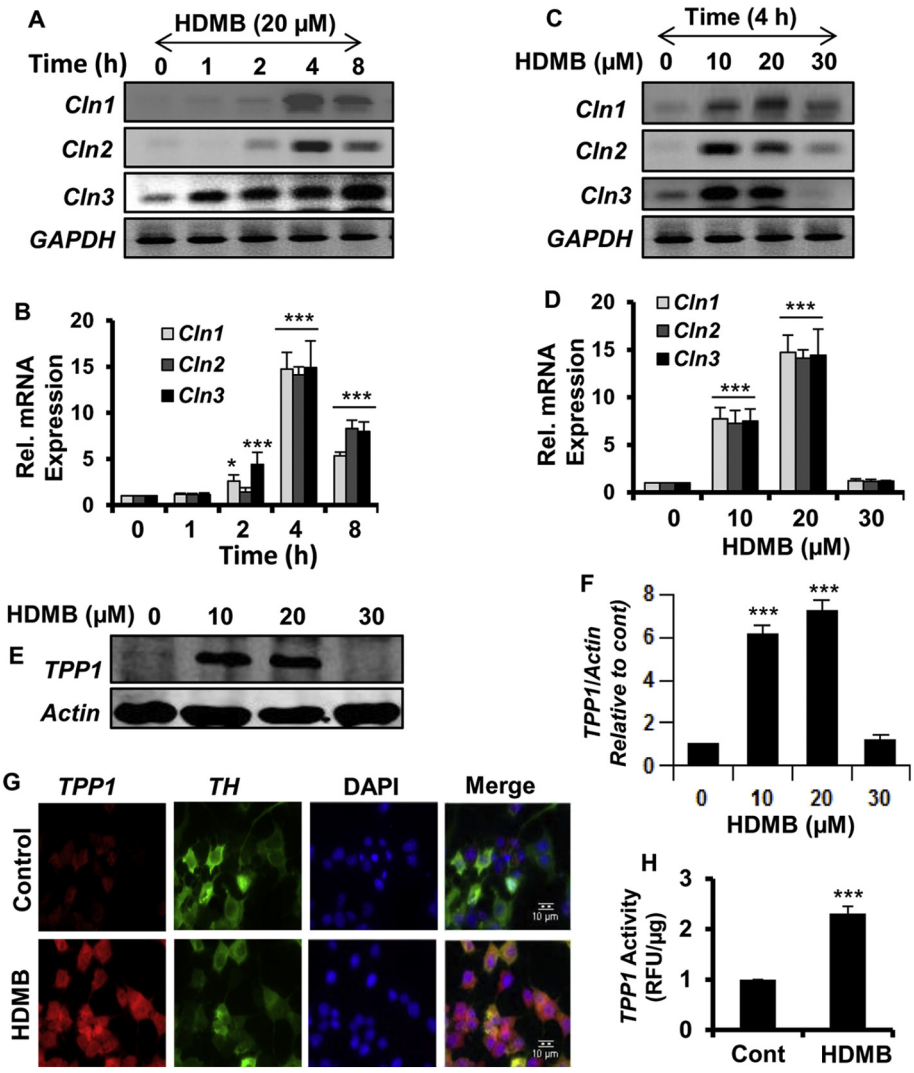

Fig. 1. HDMB upregulates TPP1 expression in MN9D neuronal cells. (A–B) For time-point analysis, MN9D cells were treated with 20 μM HDMB in neurobasal media without B27 for 1, 2, 4, and 8 h followed by monitoring the mRNA expression of *Cln1, Cln2*, and *Cln3* by semi-quantitative RT-PCR (A) and real-time qPCR (B). (C-D) For dose-dependent study, MN9D cells were treated with different concentrations of HDMB (10, 20, 30uM) for 4 h under the same culture conditions followed by monitoring the mRNA expression of *Cln1, Cln2* and *Cln3* by semi-quantitative RT-PCR (C) and real-time qPCR (D). (*E*-F) MN9D cells were treated with different concentrations of HDMB for 18 h under the same culture conditions followed by immunoblot analysis for TPP1 (E) and densitometric analysis of TPP1 expression relative to β-actin (F). (G) MN9D cells were treated with 20 μM HDMB under similar culture conditions and were double-labeled for TPP1 (red) and TH (green); Scale bar10 μm. (H) MN9D cells were treated with 20 μM HDMB under the same culture conditions for 18 h followed by TPP1 activity assay using cell extract containing 20 μg of total protein. All results are represented as mean ± SD of at least three independent experiments. $^{*}p < .05$ & $^{***}p < .001$ vs control. (For interpretation of the references to colour in this figure legend, the reader is referred to the web version of this article.)

3.4. Upregulation of TPP1 by HDMB is dependent on PPARα

To further confirm the involvement of PPARα, we analyzed the effect of HDMB on TPP1 expression in primary astrocytes isolated from wild type (WT), PPARα$^{-/-}$ and PPARβ$^{-/-}$ mice. We first checked the mRNA expression of different *Cln* genes following HDMB treatment. Interestingly, HDMB upregulated *Cln1*, *Cln2* and *Cln3* gene expressions in astrocytes isolated from WT (Fig. 4A, D) and PPARβ$^{-/-}$ (Fig. 4C, F), but not PPARα$^{-/-}$, mice (fig. B, E), indicating that HDMB specifically requires PPARα for the upregulation of these *Cln* genes. Next, we checked the protein levels of TPP1 in WT, PPARα$^{-/-}$ and PPARβ$^{-/-}$ astrocytes by immunoblotting and observed that HDMB increases TPP1 levels in WT (Fig. 4G, H) and PPARβ$^{-/-}$ (Fig. 4K, L), but not in PPARα$^{-/-}$, astrocytes (Fig. 4I, J), confirming that HDMB upregulates TPP1 via PPARα. Immunofluorescence study also demonstrated that HDMB markedly enhanced TPP1 expression in WT and PPARβ$^{-/-}$ astrocytes; however, no effect of HDMB was observed in PPARα$^{-/-}$ astrocytes (Fig. 4M). Collectively, these results establish that HDMB requires PPARα to upregulate TPP1.

3.5. Administration of HDMB increases TPP1 levels in vivo in the brain of *Cln2* $^{+/-}$ mice

After demonstrating the effect of HDMB in vitro, we next explored whether HDMB could augment TPP1 expression in the brain of transgenic mice heterozygous for Cln2 (*Cln2* $^{+/-}$ mice). The *Cln2*$^{+/-}$ mice retain one intact copy of the *Cln2* gene which makes it possible to test for potential therapeutic agents for their ability to enhance TPP1 levels in this model. *Cln2*$^{+/-}$ mice (8-weeks old) were treated with HDMB (5 mg/kg body weight/day) or vehicle (0.1% methylcellulose) for 14 days via oral gavage. First, we analyzed the mRNA expression of *Cln1*, *Cln2* and *Cln3* genes in the cortex and striatum of these mice. Semi-quantitative RT-PCR and real-time PCR data showed that HDMB treatment distinctly increased the mRNA expression of *Cln1*, *Cln2* and *Cln3* in both motor cortex (Fig. 5A, B) and striatum (Fig. 5C, D) whereas vehicle treated group did not exhibit any such effect. Next, we checked the protein levels of TPP1 and observed a remarkable increase with HDMB treatment compared to the untreated control and the vehicle-treated group both in motor cortex (Fig. 5E, F) and striatum (Fig. 5G, H). These results were further confirmed by double-labeling of TPP1 and NeuN in free-floating sections that showed distinct increase in TPP1 expression in the motor cortex (Fig. 5I) and striatum (Fig. 5J) of HDMB-treated mice. Subsequently, we analyzed the TPP1 activity in the motor cortex of these mice. HDMB-treated mice exhibited significantly higher TPP1 activity relative to the untreated control and vehicle-treated mice (Fig. 5K) indicating that oral administration of HDMB enhances the functional activity of TPP1 in *Cln2*$^{+/-}$ mice. Therefore, our results demonstrate that oral administration of HDMB augments both level and function of TPP1 in the brain of *Cln2* $^{+/-}$ mice.

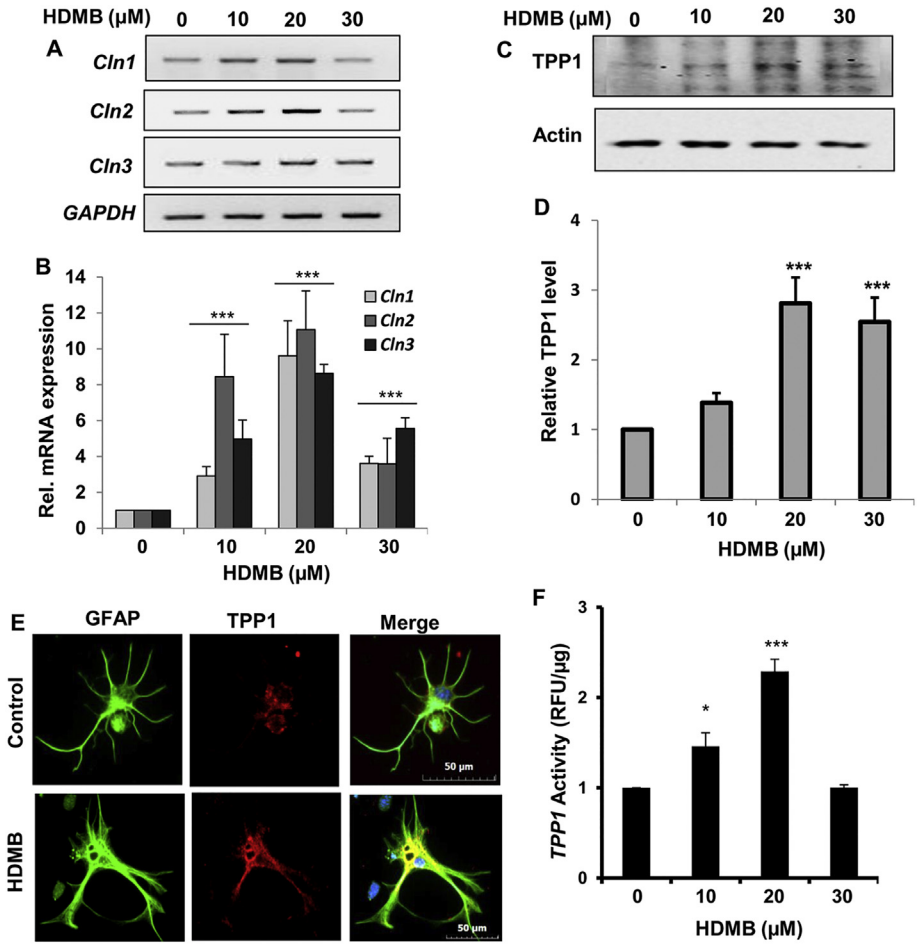

Fig. 2. HDMB enhances TPP1 expression in mouse primary astrocytes. (A–B) Wild Type (WT) mouse primary astrocytes were treated with different concentrations of HDMB in serum-free DMEM/F12 50/50 media for 4 h followed by monitoring the mRNA expression of *Cln1*, *Cln2* and *Cln3* by semi-quantitative RT-PCR (A) and real-time qPCR (B). (C–D) WT Mouse primary astrocytes were treated with different concentrations of HDMB for 18 h under the same culture conditions followed by immunoblot analysis for TPP1 (C) and densitometric analysis of *TPP1* expression relative to β-actin (D). (E) Mouse primary astrocytes were treated with 20 μM HDMB for 24 h under similar culture conditions and were double-labeled for *TPP1* (red) and *GFAP* (green). DAPI was used for staining nuclei. Scale bar = 10 μm. (F) Mouse primary astrocytes were treated with different concentrations of HDMB (10, 20, 30 μM) in serum-free DMEM /F12 50/50 media for 18 h followed by the *TPP1* activity assay using cell extract containing 20 μg of total protein. All results represent mean ± SD of at least three independent experiments. $^{*}p < .05$ & $^{***}p < .001$ vs control. (For interpretation of the references to colour in this figure legend, the reader is referred to the web version of this article.)

3.6. HDMB-mediated upregulation of TPP1 is abrogated in the absence of PPARα

Next, we explored whether HDMB-mediated upregulation of TPP1 is dependent on PPARα. In this regard, we generated a mouse model which was heterozygous for Cln2 and null for PPARα (*Cln2*$^{+/-}$*PPARα*$^{-/-}$) by crossing *Cln2*$^{-/-}$ mice with *PPARα*$^{-/-}$ mice. We used two months old *Cln2*$^{+/-}$ *PPARα*$^{-/-}$ mice (n = 5/group) for HDMB treatment. As expected, *Cln2*$^{+/-}$ mice presented significantly less amount of TPP1 in the motor cortex compared to the WT mice; however, oral administration of HDMB significantly upregulated TPP1 levels in the motor cortex of *Cln2*$^{+/-}$ mice (Fig. 6A, B). Interestingly, when we compared *Cln2*$^{+/-}$ and *Cln2*$^{+/-}$*PPARα*$^{-/-}$ mice, we observed that unlike *Cln2*$^{+/-}$ mice, HDMB was unable to upregulate TPP1 in the motor cortex of *Cln2*$^{+/-}$*PPARα*$^{-/-}$ mice (Fig. 6C, D), indicating that HDMB does not exhibit any effect in the absence of PPARα. In parallel to our immunoblot results, double-labeling of TPP1 and NeuN in the motor cortex revealed that *Cln2*$^{+/-}$ mice have distinctly lower number of TPP1 positive cells compared to the WT control. Importantly, oral administration of HDMB remarkably increased the TPP1 levels in *Cln2*$^{+/-}$, but not in *Cln2*$^{+/-}$*PPARα*$^{-/-}$, mice (Fig. 6E, F), further confirming that the effect of HDMB is abolished in the absence of PPARα. Accordingly, HDMB treatment also increased the activity of TPP1 in the motor cortex of *Cln2*$^{+/-}$, but not in *Cln2*$^{+/-}$*PPARα*$^{-/-}$, mice (Fig. 6G). Taken together, these results establish that HDMB upregulates TPP1 in the brain of *Cln2*$^{+/-}$ mice via PPARα. We did not notice any side effect (e.g. hair loss, weight loss, diarrhea, untoward infection, etc.) in any of the mice during HDMB treatment.

3.7. HDMB treatment stimulates the recruitment of PPARα, but neither PPARβ nor PPARγ, to the Cln2 gene promoter

Finally, we intended to characterize the mechanism how exactly activation of PPARα by HDMB regulates Cln2 expression. Previously, we reported the presence of a RXR-binding site on the *Cln2* gene promoter (depicted in Fig. 7A) and established that the PPARα-RXRα heterodimer transcriptionally upregulates the expression of *Cln2* (Ghosh et al., 2012). Hence, we checked whether HDMB treatment recruits PPARα to the *Cln2* promoter by performing chromatin immunoprecipitation in MN9D neuronal cells. Following 2 h of treatment with HDMB, the sheered chromatin was immunoprecipitated with antibodies against PPARα, RXRα, PPARβ, PPARγ, and PGC1α. Semi-quantitatve PCR data showed that HDMB selectively recruited PPARα, RXRα and PGC1α, but neither PPARβ nor PPARγ, to the *Cln2* promoter (Fig. 7B). Real-time PCR data showed a similar pattern of increase in PPARα, RXRα and PGC1α (Fig. 7C), further confirming that HDMB promotes the formation of a transcriptional complex containing PPARα, RXRα and PGC1α on the *Cln2* promoter which positively regulates the expression of the *Cln2* gene. These data directly demonstrate that HDMB-mediated PPARα activation transcriptionally upregulates TPP1.

4. Discussion

Current therapeutic approaches for the treatment of NCLs are focused on delivery of functional copy of the gene, stem cells or recombinant enzyme to the brain which, although have promising outcomes, are extensively invasive and expensive. Hence, there is a necessity for a novel, minimally or non-invasive and economic treatment strategies for these fatal childhood disorders. The classic late-

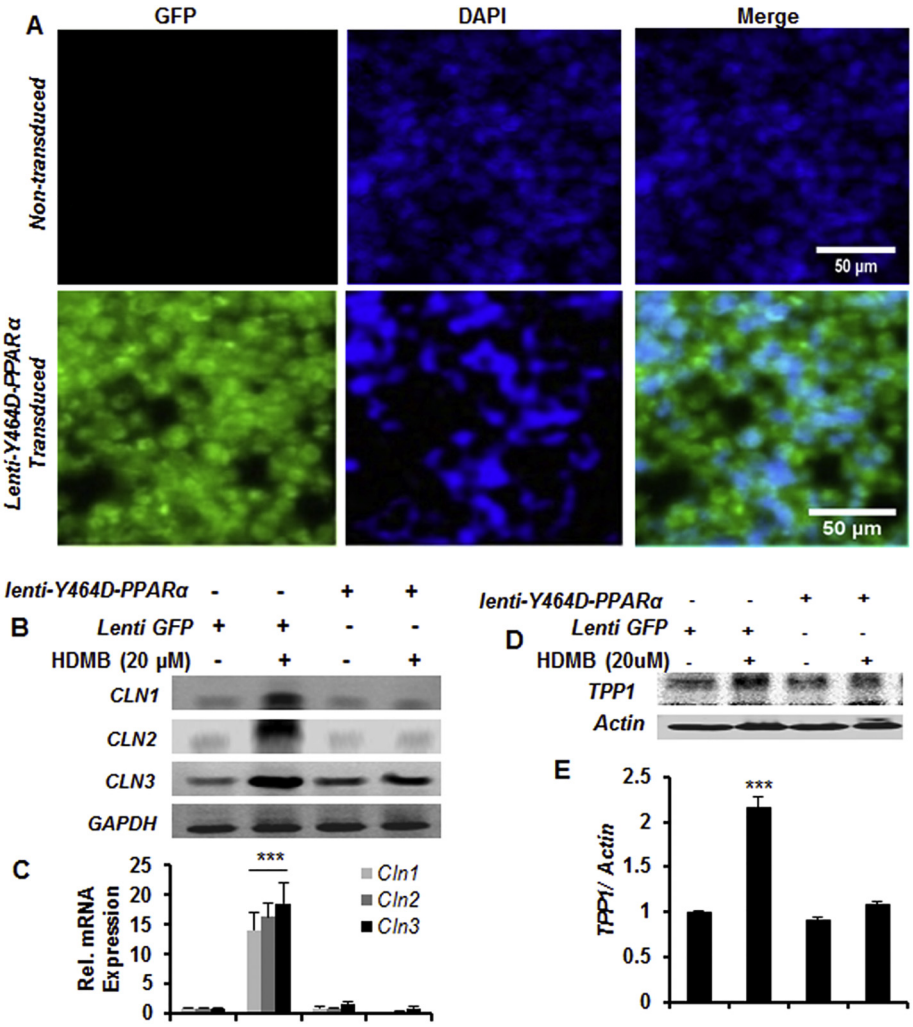

Fig. 3. HDMB requires PPARα for increasing TPP1 expression. (A–E) MN9D cells were transduced with *Lenti-Y464D-PPARα* construct or *Lenti-GFP* for 48 h. Fig. 3A shows the transduction efficiency in MN9D cells compared to non-transduced cells; DAPI was used to stain the nuclei (A). Transduced cells were treated with 20 μM HDMB for 4 h followed by monitoring the mRNA expression of *Cln1, Cln2*, and *Cln3* by semi-quantitative RT-PCR (B) and real-time qPCR (C). *Lenti-Y464D-PPARα* or *Lenti-GFP* transduced cells were treated with 20 μM of HDMB for 18 h followed by immunoblot for TPP1 (D) and densitometric analysis of TPP1 expression relative to β-actin (E). All results are represented as mean ± SD of at least three independent experiments. $^{***}p < .001$ vs control.

infantile form of NCL (LINCL) is characterized by mutations in the *Cln2* gene, which encodes a lysosomal enzyme TPP1. Several reports have indicated that residual activity of TPP1 is retained in LINCL (Sleat et al., 1999; Viglio et al., 2001; Walus et al., 2010) prompting a new field of research directed towards enhancing the function of residual TPP1 under disease scenario. In this study, we demonstrate that HDMB, an endogenous ligand of PPARα, can upregulate TPP1 expression and activity in mouse neuronal cell line and primary brain cells. We also established that the effect of HDMB was specifically mediated by activation of the nuclear receptor PPARα. Importantly, administration of HDMB to the heterozygous *Cln2*$^{+/-}$ mice markedly enhanced TPP1 levels in motor cortex and striatum in a PPARα-dependent fashion. Finally, we delineate that recruitment of PPARα and formation of a transcriptional complex on the *Cln2* gene promoter is the underlying mechanism of HDMB-mediated TPP1 upregulation. Therefore, administration of HDMB might be beneficial for the treatment of LINCL patients.

PPARs are ligand inducible transcription factors that act as lipid sensors. One of the isoforms, PPARα, is primarily involved in energy homeostasis although it has been reported to modulate several other physiological processes (Heneka and Landreth, 2007; Heneka et al., 2011). Our lab has established that PPARα is involved in memory improvement via targeting the CREB signaling pathway (Roy et al., 2013). We have also demonstrated that acivation of PPARα induces lysosomal biogenesis in brain cells through transcriptional upregulation of the master regulator TFEB (Ghosh et al., 2015). Importantly, activation of PPARα by fibrate drugs was observed to stimulate TPP1 expression via forming heterodimer with RXRα (Ghosh et al., 2012). Owing to the immense implications of this hormone receptor in physiological and pathological processes, endogenous ligands of PPARα could be highly beneficial as therapeutic agents. In this study, we demonstrate that HDMB induces TPP1 expression in brain cells as well as in vivo in the brain of a disease model for LINCL (*Cln2*$^{+/-}$) via PPARα.

In a recent study by our group, HDMB was detected as an endogenous molecule that binds to the ligand-binding domain of PPARα in the mouse hippocampus and was reported to stimulate synaptic functions (Roy et al., 2016). The Tyr464 (Y464) was identified as an active site residue in the ligand-binding domain of PPARα which was important for binding of HDMB (Roy et al., 2016). In this study, as expected, when a dominant-negative construct of PPARα (Y464D) was used, the effect of HDMB on TPP1 upregulation was abolished. This confirmed that HDMB specifically requires the binding to the PPARα ligand-binding domain for inducing TPP1 expression.

While examining the mechanisms underlying HDMB-mediated upregulation of TPP1, we observed that HDMB transcriptionally enhances *Cln2* expression via PPARα. PPARs contain four functional domains including a ligand-binding domain and a highly conserved DNA-binding domain (Heneka and Landreth, 2007; Heneka et al., 2011). Under unstimulated conditions, PPARs are sequestered in the cytosol by binding to corepressor molecules. Activation of the receptor upon ligand-binding leads to dissociation from the corepressor complex, binding of coactivators and formation of heterodimer with RXRs. The PPAR-RXR transcriptional complex binds to the PPRE (peroxisome-proliferator response elements) sequence on the promoter of target

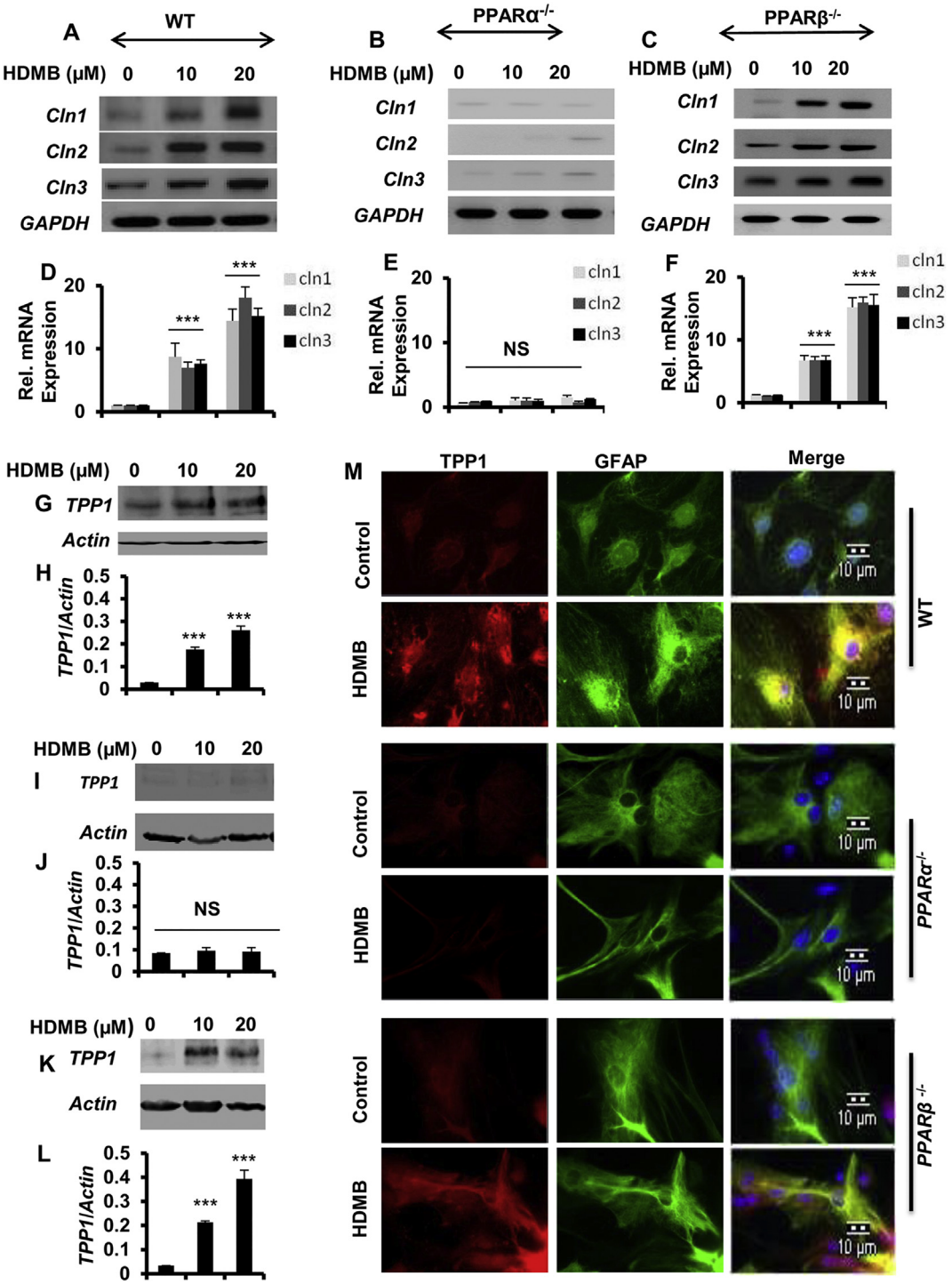

Fig. 4. Upregulation of TPP1 by HDMB is dependent on PPARα. (A–F) Mouse primary astrocytes isolated from Wild Type (WT), *PPARα*$^{-/-}$ and *PPARβ*$^{-/-}$ mice were treated with different concentrations of HDMB in serum-free DMEM/F-12, 50/50 media for 4 h followed by monitoring the mRNA expression of *Cln1, Cln2* and *Cln3* genes by semi-quantitative RT-PCR (A, B, C) and real-time qPCR (D, E, F). (G-L) WT, *PPARα*$^{-/-}$ and *PPARβ*$^{-/-}$ mouse primary astrocytes were treated with different concentrations of HDMB under serum free conditions for 18 h followed by immunoblot analysis of TPP1 and densitometric analysis of TPP1 expression relative to β-actin (G,H for WT; I,J for *PPARα*$^{-/-}$ and K,L for *PPARβ*$^{-/-}$). (M) Mouse primary astrocytes isolated from WT, *PPARα*$^{-/-}$ and *PPARβ*$^{-/-}$ mice were treated with 20 μM HDMB in serum-free DMEM/F-12, 50/50 media for 18 h and double-labeled for *TPP1* (red) and *GFAP* (green). DAPI was used for staining nuclei; Scale bar = 10 μm. (M). All results are represented as mean ± SD of at least three independent experiments. ***$p < .001$ vs control. (For interpretation of the references to colour in this figure legend, the reader is referred to the web version of this article.)

gene to regulate gene expression (Heneka and Landreth, 2007; Heneka et al., 2011). Promoter analysis of mouse *Cln2* gene revealed no PPRE site; however, RXR-binding site was observed in the promoter region upstream of the transcription start site (−687 to −663 bp) (Ghosh et al., 2012). We have previously demonstrated that PPARα agonist gemfibrozil leads to recruitment of PPARα-RXRα complex to the RXR-binding site on the *Cln2* gene promoter (Ghosh et al., 2012). In this study, we observed that HDMB treatment leads to the recruitment of PPARα, RXRα and PGC1α to the RXR-binding site on *Cln2* promoter to transcriptionally upregulate *Cln2* gene expression.

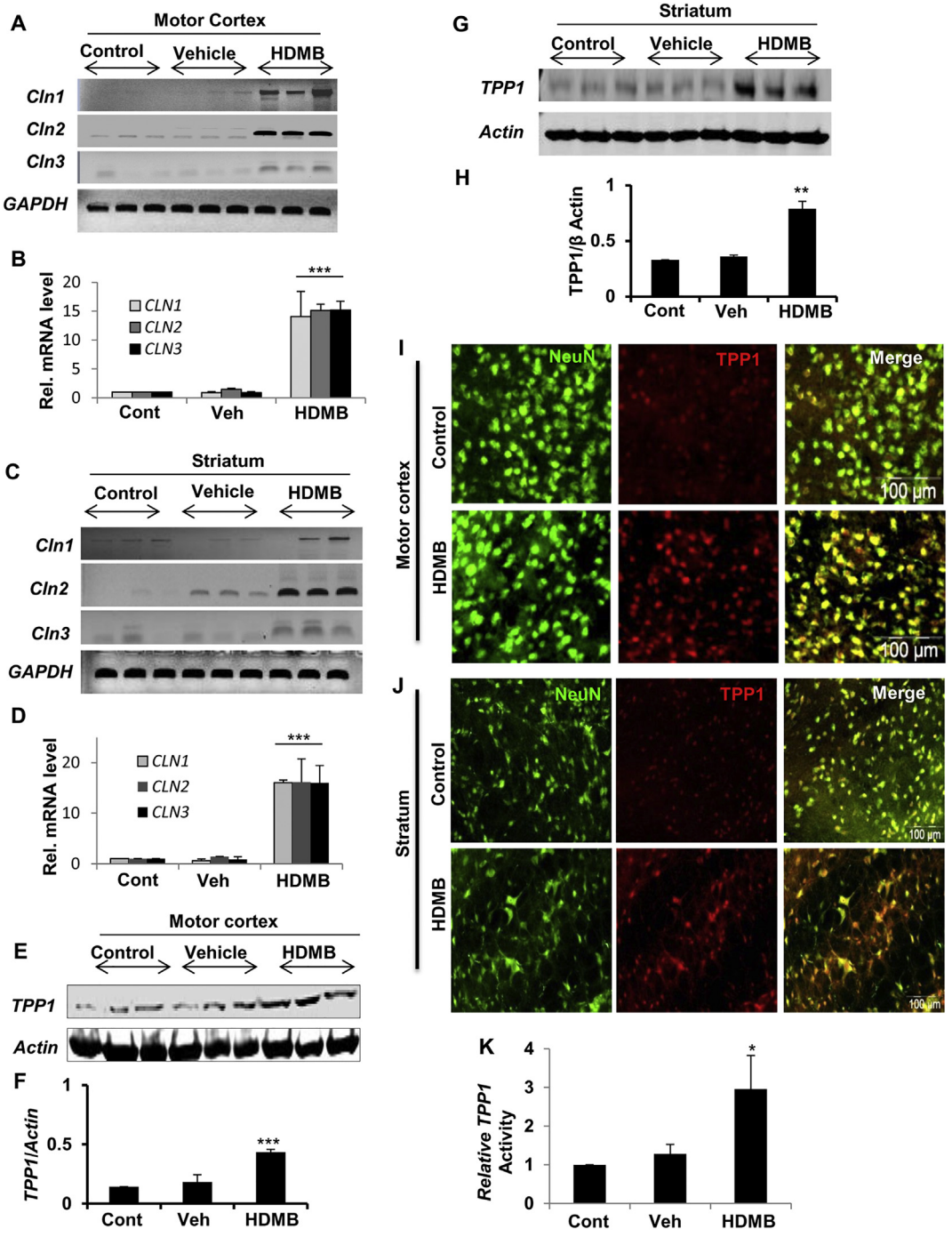

Fig. 5. Administration of HDMB increases TPP1 levels in vivo in the brain of *Cln2* $^{+/-}$ mice. (A–D) 8-weeks old *Cln2*$^{+/-}$ mice (n = 5 in each group) were treated with 5 mg/kg body weight/day HDMB (dissolved in 0.1% methylcellulose) or vehicle (0.1% methylcellulose) via oral gavage. After 14 days of treatment, untreated, vehicle-treated and HDMB-treated mice were sacrificed and the motor cortex and striatum were dissected. The mRNA expression of *Cln1, Cln2* and *Cln3* were monitored by semi-quantitative RT-PCR and real-time qPCR in cortex (A, B) and striatum (C, D). (E–H) Immunoblot and densitometric analysis of TPP1 expression in the motor cortex (E, F) and striatum (G, H). (I–J) Double labeling of TPP1 and NeuN in Cortical (I) and Striatal (J) free floating sections; Data represent analysis of three cortical and striatal sections from each of four different mice per group. Scale bar = 100 µm. (K) TPP1 was assayed from mouse cortical homogenate as described under Methods section and presented as relative to control. Control TPP1 activity represents 0.9 ± 0.2 nmol/mg protein. Results are mean ± SEM of five mice per group. $^{*}p < .05$, $^{**}p < .01$ & $^{***}p < .001$ vs untreated control.

Our cell culture studies revealed that along with Cln2, HDMB also enhanced the expression of lysosomal genes *Cln1* and *Cln3* in the MN9D neuronal cell line and in mouse primary astrocytes. The gene *Cln1*, located on chromosome 1p34.2, encodes the enzyme PPT1 (palmitoyl protein thioesterase 1) which eliminates palmitate groups from its substrate proteins. Mutations in *Cln1* lead to PPT1 deficiency resulting in classic infantile NCL or Haltia-Santavuori disease (Nita et al., 2016; Warrier et al., 2013; Haltia, 2006). The *Cln3* gene is mapped to 16p11.2 and encodes a membrane protein Cln3, which when mutated causes juvenile NCL or Batten-Spielmeyer-Sjögren disease (Nita et al., 2016; Warrier et al., 2013; Haltia, 2006). We have observed that HDMB increases the mRNA expression of both *Cln1* and *Cln3* in a dose-dependent manner. These results suggest that HDMB might have therapeutic implications for Infantile NCL (INCL) and Juvenile NCL (JNCL) as well.

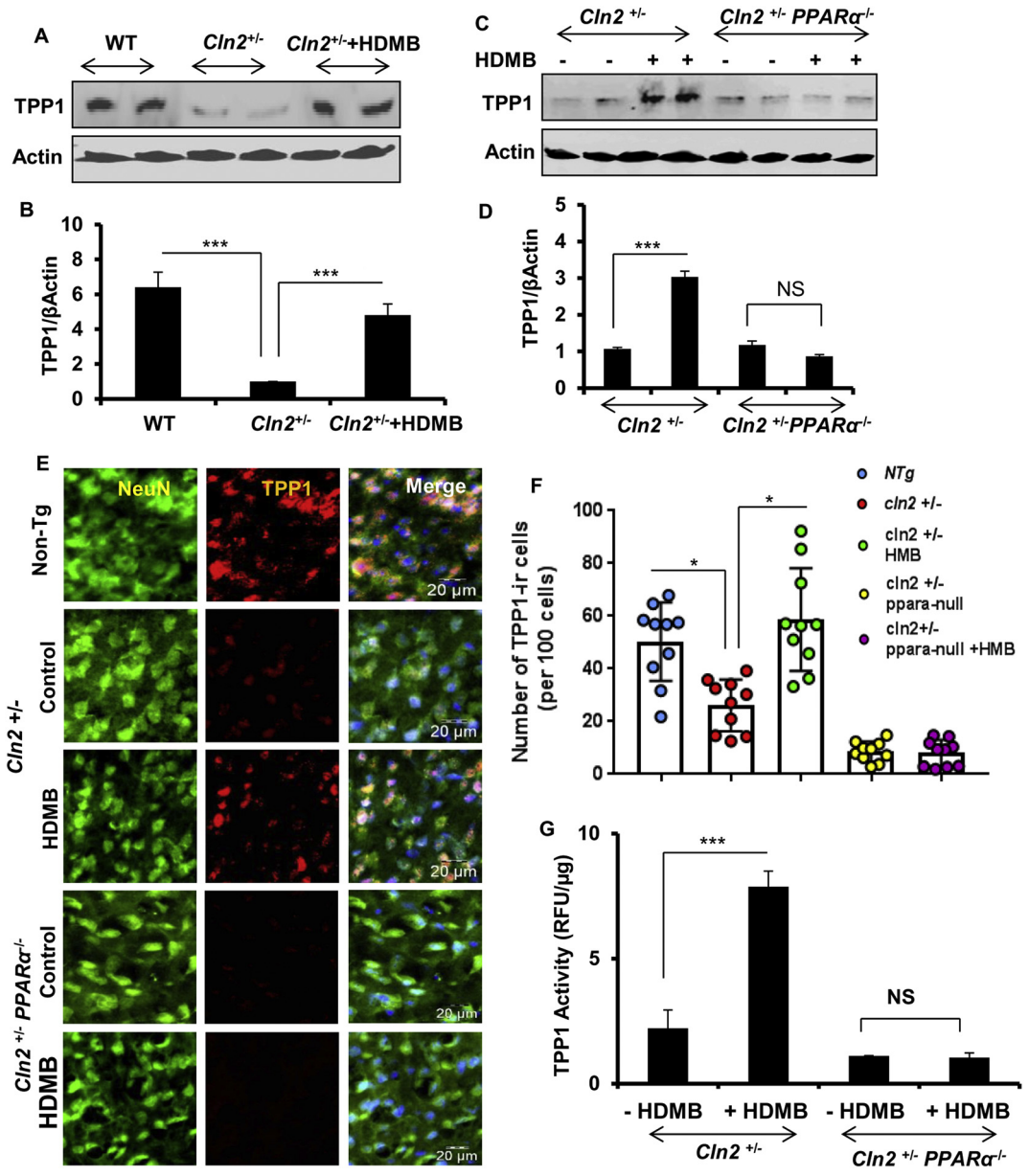

Fig. 6. HDMB-mediated upregulation of TPP1 is abrogated in the absence of PPARα. (A–G) 8-weeks old *Cln2*$^{+/-}$ and *Cln2*$^{+/-}$*PPARα*$^{-/-}$ mice (n = 5 in each group) were treated with 5 mg/kg body weight/day HDMB (dissolved in 0.1% methylcellulose) or vehicle (0.1% methylcellulose) for 14 days via oral gavage. Untreated WT mice were used as a control for basal endogenous levels of TPP1. Immunoblot analysis for TPP1 expression in the motor cortex of WT and *Cln2*$^{+/-}$ untreated control and *Cln2*$^{+/-}$ HDMB treated mice (B) and densitometric analysis (relative to β-actin) (C). Immunoblot analysis of TPP1 expression in untreated and HDMB treated *Cln2*$^{+/-}$ and *Cln2*$^{+/-}$*PPARα*$^{-/-}$ mice (D) and densitometric analysis (E). Double-labeling of motor cortex from untreated and HDMB treated *Cln2*$^{+/-}$ and *Cln2*$^{+/-}$ *PPARα*$^{-/-}$ mice with TPP1 (red) and NeuN (green). DAPI was used for staining the nuclei. Scale bar = 20 µm (F). Quantification of number of TPP1-immunoreactive cells per 100 cells in the motor cortex (G). Data represents analysis of three cortical sections from each of five different mice per group. TPP1 activity assay from cortex of untreated and treated *Cln2*$^{+/-}$ and *Cln2*$^{+/-}$*PPARα*$^{-/-}$ mice (H). Results are mean ± SEM of five mice per group. $^{*}p < .05$ & $^{***}p < .001$. (For interpretation of the references to colour in this figure legend, the reader is referred to the web version of this article.)

Several mutations have been associated with the *Cln2* gene that results in loss or deficiency of TPP1 activity. The three most common mutations observed in most LINCL cases are an intron G to C transversion in the 3′ splice junction of intron 5 (3556G-C); an exon 6C to T transversion that prematurely stops translation (3670C-T; Arg 208Stop); and a missense mutation G to C in exon 10 (5271G-C; Gln422His) (Sondhi et al., 2001; Crystal et al., 2004). Many of the missense mutations observed in TPP1 are associated with abnormal folding of the mutant protein resulting in extended half-life of pro-TPP1 or inefficient trafficking to the lysosomes resulting in lower activity of the enzyme (Walus et al., 2010). However, several TPP1 variants have been observed to response to permissive temperature and chemical chaperone treatment indicating that folding enhancement could be an effective strategy to rescue the function of some variant of TPP1 (Walus et al., 2010).

Mounting evidence indicate that residual TPP1 activity is retained in LINCL patients and can be targeted for therapeutic strategies (Sleat et al., 1999; Viglio et al., 2001; Walus et al., 2010). Indeed, low levels of TPP1 activity was observed in the lymphocytes from LINCL patients by a capillary electrophoresis technique (Viglio et al., 2001). Similar to this, residual TPP1 activity was also reported in biological samples from LINCL patients as well as different animal model using an enzyme-based assay (Sohar et al., 1999). An Arg447His missense mutation associated with late age of onset and clinically protracted course of the disease

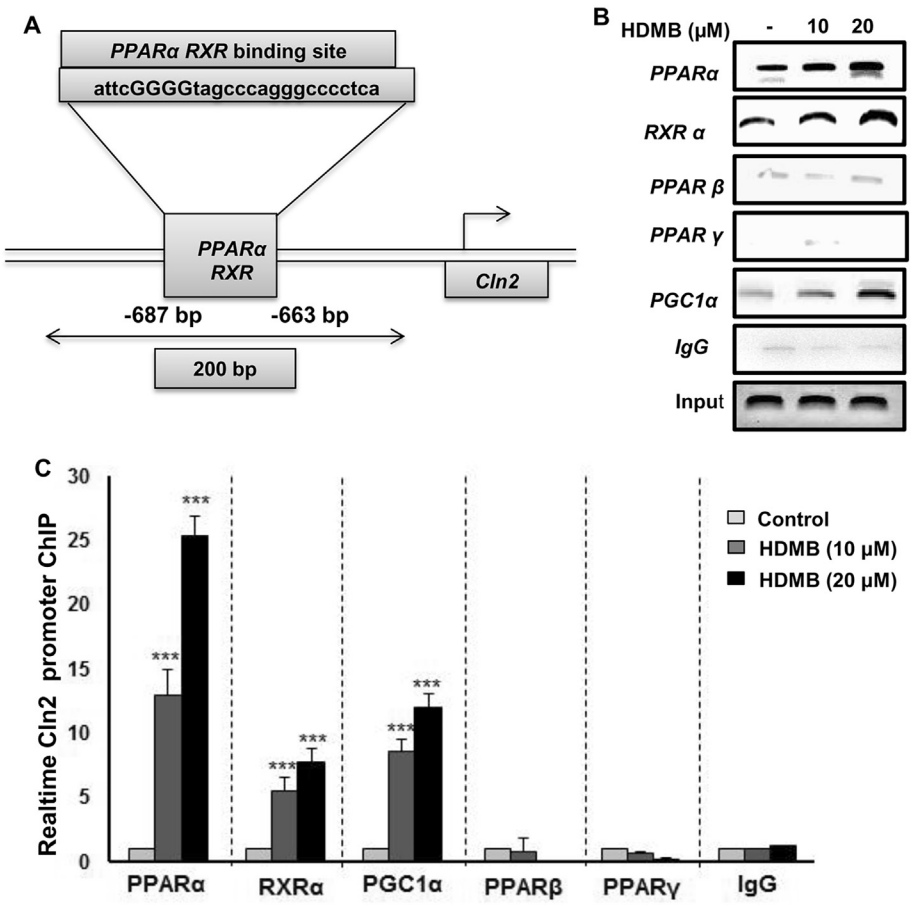

Fig. 7. HDMB stimulates the recruitment of PPARα to the *Cln2* gene promoter. MN9D neuronal cells were treated with 10 and 20 μM HDMB under serum free conditions for 2 h following which the nuclear extract was subjected to chromatin immunoprecipitation. Recruitment of PPARα, RXRα, PPARβ, PPARγ, and PGC1α on the *RXR*-binding site of *Cln2* promoter (A) was monitored by semi-quantitative PCR (B) and real-time qPCR (C). IgG was used as a control. All results are represented as mean ± SD of at least three independent experiments. $^{***}p < .001$ vs control.

suggests that restoration of low levels of normal TPP1 activity might be adequate and result in a much milder form of the disease (Sleat et al., 1999; Sondhi et al., 2001). An interesting study on CLN2 mutant mice expressing variant amounts of residual TPP1 activity found that 3% of regular TPP1 activity is sufficient to delay the onset and double the lifespan whereas 6% normal TPP1 activity results in attenuation of the disease and remarkably improved lifespan of the mice indicating 6% functional TPP1 activity. Therefore, therapies targeted at achieving as low as 6% of TPP1 functionality in the CNS might be beneficial for LINCL patients (Sleat et al., 2008).

The Cln2 targeted mutant mice ($Cln2^{-/-}$) successfully recapitulates many of the LINCL characteristics including tremor, ataxia, neuronal pathology marked by lysosomal storage material, axonal degeneration and reduced lifespan (Sleat et al., 2004). In a previous study, we demonstrated that Gemfibrozil, a FDA approved PPARα agonist, increased the lifespan of $Cln2^{-/-}$ model of LINCL (Ghosh et al., 2017). Gemfibrozil-treated mice had reduced burden of storage granules, enhanced expression of anti-inflammatory and anti-apoptotic factors and lowered neuronal apoptosis compared to vehicle treated $Cln2^{-/-}$ mice (Ghosh et al., 2017). In this study, we used Cln2 heterozygous mice ($Cln2^{+/-}$) which have one normal copy of the Cln2 gene providing opportunity to test drug-mediated regulation of TPP1 in this model. Marked increase in TPP1 in the motor cortex of $Cln2^{+/-}$, but not $Cln2^{+/-}PPAR\alpha^{-/-}$, mice by HDMB suggests that HDMB requires PPARα to upregulate the expression of TPP1 in $Cln2^{+/-}$ mice.

Gene therapy, enzyme replacement therapy and stem cell transplantation have shown promising results for the treatment of LINCL (Worgall et al., 2008; Xu et al., 2011; Chang et al., 2008; Vuillemenot et al., 2011; Sondhi et al., 2007; Sondhi et al., 2008; Cabrera-Salazar et al., 2007; Hackett et al., 2005; Selden et al., 2013). These therapies are targeted at delivery of active TPP1 in adequate amount to counter the cell loss observed in LINCL (Sondhi et al., 2001). In vivo gene therapy involves delivery of a vector containing the human *Cln2* cDNA to the CNS and retinal cells in LINCL patients. Although it has demonstrated efficacy in animal models and human patients (Worgall et al., 2008; Sondhi et al., 2007; Sondhi et al., 2008; Cabrera-Salazar et al., 2007; Hackett et al., 2005), several factors makes it challenging to evolve as a widely applicable therapy. In order to succeed, firstly, substantial amount of the active TPP1 protein has to be produced to reach the therapeutic levels. Secondly, since LINCL is a genetic disorder, the active TPP1 protein has to be produced for long duration and will need subsequent delivery of the vector. Thirdly, the gene delivery has to target an extensive brain region so that the protein can spread through the affected cells (Sondhi et al., 2001; Sondhi et al., 2007). In enzyme augmentation therapy, recombinant TPP1 protein is directly infused into the brain of LINCL patients. However, purification of recombination enzyme and the need for continuous administration of the protein pose several difficulties (Sondhi et al., 2001). A recent study showed that enzyme augmentation therapy via intraventricular infusion of cerliponase alfa (recombinant human pro-TPP1) reduces the impairment of locomotor and language functions in children affected with CLN2 disease (Schulz et al., 2018). The study involved infusion of the recombinant protein every 2 weeks for 240 weeks in children of 3 to 16 years age. Although this is the first FDA-approved therapy for LINCL, the repeated administration of intraventricular device is fairly invasive and expensive. Moreover, the treatment led to adverse side effects including development of infections from the device (Schulz et al., 2018). Therefore, a drug-mediated therapeutic strategy using HDMB could be advantageous than prospective treatments for LINCL due to several factors. HDMB is an endogenous molecule and therefore will be well-tolerated by the body and have minimal toxicities. Finally, HDMB can be delivered orally which is the least painful route for treatment and is

suitable for children.

In summary, this study demonstrates that HDMB, an endogenous ligand of PPARα, can upregulate TPP1. We delineate that HDMB activates the nuclear receptor PPARα to enhance TPP1 expression. Furthermore, we showed that HDMB recruits the PPARα-RXRα heterodimer complex to the *Cln2* gene promoter to transcriptionally regulate the expression. Moreover, in *Cln2*$^{+/-}$ mice, oral administration of HDMB leads to enhanced TPP1 expression in the motor cortex and striatum. Therefore, HDMB may have therapeutic potential for LINCL.

Acknowledgements

This study was supported by a grant from National Institutes of Health (AG050431) and a merit award from Veteran Affairs (1I01BX003033).

References

Brahmachari, S., Pahan, K., 2007. Sodium benzoate, a food additive and a metabolite of cinnamon, modifies T cells at multiple steps and inhibits adoptive transfer of experimental allergic encephalomyelitis. J. Immunol. 179, 275–283.

Cabrera-Salazar, M.A., Roskelley, E.M., Bu, J., Hodges, B.L., Yew, N., Dodge, J.C., Shihabuddin, L.S., Sohar, I., Sleat, D.E., Scheule, R.K., Davidson, B.L., Cheng, S.H., Lobel, P., Passini, M.A., 2007. Timing of therapeutic intervention determines functional and survival outcomes in a mouse model of late infantile batten disease. Mol. Ther. 15, 1782–1788.

Chang, M., Cooper, J.D., Sleat, D.E., Cheng, S.H., Dodge, J.C., Passini, M.A., Lobel, P., Davidson, B.L., 2008. Intraventricular enzyme replacement improves disease phenotypes in a mouse model of late infantile neuronal ceroid lipofuscinosis. Mol. Ther. 16, 649–656.

Corbett, G. T., Roy, A., and Pahan, K. Gemfibrozil, a lipid-lowering drug, upregulates IL-1 receptor antagonist in mouse cortical neurons: implications for neuronal self-defense. J. Immunol. 189, 1002–1013.

Crystal, R.G., Sondhi, D., Hackett, N.R., Kaminsky, S.M., Worgall, S., Stieg, P., Souweidane, M., Hosain, S., Heier, L., Ballon, D., Dinner, M., Wisniewski, K., Kaplitt, M., Greenwald, B.M., Howell, J.D., Strybing, K., Dyke, J., Voss, H., 2004. Clinical protocol. Administration of a replication-deficient adeno-associated virus gene transfer vector expressing the human CLN2 cDNA to the brain of children with late infantile neuronal ceroid lipofuscinosis. Hum. Gene Ther. 15, 1131–1154.

Dasgupta, S., Jana, M., Zhou, Y., Fung, Y.K., Ghosh, S., Pahan, K., 2004. Antineuroinflammatory effect of NF-kappaB essential modifier-binding domain peptides in the adoptive transfer model of experimental allergic encephalomyelitis. J. Immunol. 173, 1344–1354.

Ghosh, A., Corbett, G.T., Gonzalez, F.J., Pahan, K., 2012. Gemfibrozil and fenofibrate, Food and Drug Administration-approved lipid-lowering drugs, up-regulate tripeptidyl-peptidase 1 in brain cells via peroxisome proliferator-activated receptor alpha: implications for late infantile Batten disease therapy. J. Biol. Chem. 287, 38922–38935.

Ghosh, A., Jana, M., Modi, K., Gonzalez, F.J., Sims, K.B., Berry-Kravis, E., Pahan, K., 2015. Activation of peroxisome proliferator-activated receptor alpha induces lysosomal biogenesis in brain cells: implications for lysosomal storage disorders. J. Biol. Chem. 290, 10309–10324.

Ghosh, A., Rangasamy, S.B., Modi, K.K., Pahan, K., 2017. Gemfibrozil, food and drug administration-approved lipid-lowering drug, increases longevity in mouse model of late infantile neuronal ceroid lipofuscinosis. J. Neurochem. 141, 423–435.

Giulian, D., Baker, T.J., 1986. Characterization of ameboid microglia isolated from developing mammalian brain. J. Neurosci. 6, 2163–2178.

Golabek, A.A., Kida, E., Walus, M., Wujek, P., Mehta, P., Wisniewski, K.E., 2003. Biosynthesis, glycosylation, and enzymatic processing in vivo of human tripeptidyl-peptidase I. J. Biol. Chem. 278, 7135–7145.

Hachiya, Y., Hayashi, M., Kumada, S., Uchiyama, A., Tsuchiya, K., Kurata, K., 2006. Mechanisms of neurodegeneration in neuronal ceroid-lipofuscinoses. Acta Neuropathol. 111, 168–177.

Hackett, N.R., Redmond, D.E., Sondhi, D., Giannaris, E.L., Vassallo, E., Stratton, J., Qiu, J., Kaminsky, S.M., Lesser, M.L., Fisch, G.S., Rouselle, S.D., Crystal, R.G., 2005. Safety of direct administration of AAV2(CU)hCLN2, a candidate treatment for the central nervous system manifestations of late infantile neuronal ceroid lipofuscinosis, to the brain of rats and nonhuman primates. Hum. Gene Ther. 16, 1484–1503.

Haines, J.L., Boustany, R.M., Alroy, J., Auger, K.J., Shook, K.S., Terwedow, H., Lerner, T.J., 1998. Chromosomal localization of two genes underlying late-infantile neuronal ceroid lipofuscinosis. Neurogenetics 1, 217–222.

Haltia, M., 2003. The neuronal ceroid-lipofuscinoses. J. Neuropathol. Exp. Neurol. 62, 1–13.

Haltia, M., 2006. The neuronal ceroid-lipofuscinoses: from past to present. Biochim. Biophys. Acta 1762, 850–856.

Heneka, M.T., Landreth, G.E., 2007. PPARs in the brain. Biochim. Biophys. Acta 1771, 1031–1045.

Heneka, M.T., Reyes-Irisarri, E., Hull, M., Kummer, M.P., 2011. Impact and therapeutic potential of PPARs in Alzheimer's disease. Curr. Neuropharmacol. 9, 643–650.

Khasnavis, S., Jana, A., Roy, A., Mazumder, M., Bhushan, B., Wood, T., Ghosh, S., Watson, R., and Pahan, K. Suppression of nuclear factor-kappaB activation and inflammation in microglia by physically modified saline. J. Biol. Chem. 287, 29529–29542.

Khasnavis, S., and Pahan, K. Sodium benzoate, a metabolite of cinnamon and a food additive, upregulates neuroprotective Parkinson disease protein DJ-1 in astrocytes and neurons. J. NeuroImmune Pharmacol. 7, 424–435.

Lane, S.C., Jolly, R.D., Schmechel, D.E., Alroy, J., Boustany, R.M., 1996. Apoptosis as the mechanism of neurodegeneration in Batten's disease. J. Neurochem. 67, 677–683.

Liu, C.G., Sleat, D.E., Donnelly, R.J., Lobel, P., 1998. Structural organization and sequence of CLN2, the defective gene in classical late infantile neuronal ceroid lipofuscinosis. Genomics 50, 206–212.

Mole, S.E., Cotman, S.L., 2015. Genetics of the neuronal ceroid lipofuscinoses (Batten disease). Biochim. Biophys. Acta 1852, 2237–2241.

Nelson, J.D., Denisenko, O., Bomsztyk, K., 2006. Protocol for the fast chromatin immunoprecipitation (ChIP) method. Nat. Protoc. 1, 179–185.

Nita, D.A., Mole, S.E., Minassian, B.A., 2016. Neuronal ceroid lipofuscinoses. Epileptic Disord 18, 73–88.

Roy, A., Jana, M., Corbett, G.T., Ramaswamy, S., Kordower, J.H., Gonzalez, F.J., Pahan, K., 2013. Regulation of cyclic AMP response element binding and hippocampal plasticity-related genes by peroxisome proliferator-activated receptor alpha. Cell Rep. 4, 724–737.

Roy, A., Kundu, M., Jana, M., Mishra, R.K., Yung, Y., Luan, C.H., Gonzalez, F.J., Pahan, K., 2016. Identification and characterization of PPARalpha ligands in the hippocampus. Nat. Chem. Biol. 12, 1075–1083.

Saha, R.N., Liu, X., Pahan, K., 2006. Up-regulation of BDNF in astrocytes by TNF-alpha: a case for the neuroprotective role of cytokine. J. NeuroImmune Pharmacol. 1, 212–222.

Saha, R.N., Pahan, K., 2007. Differential regulation of Mn-superoxide dismutase in neurons and astroglia by HIV-1 gp120: implications for HIV-associated dementia. Free Radic. Biol. Med. 42, 1866–1878.

Schulz, A., Ajayi, T., Specchio, N., de Los Reyes, E., Gissen, P., Ballon, D., Dyke, J.P., Cahan, H., Slasor, P., Jacoby, D., Kohlschutter, A., Group, C. L. N. S, 2018. Study of intraventricular cerliponase Alfa for CLN2 disease. N. Engl. J. Med. 378, 1898–1907.

Schulz, A., Kohlschutter, A., Mink, J., Simonati, A., Williams, R., 2013. NCL diseases – clinical perspectives. Biochim. Biophys. Acta 1832, 1801–1806.

Selden, N.R., Al-Uzri, A., Huhn, S.L., Koch, T.K., Sikora, D.M., Nguyen-Driver, M.D., Guillaume, D.J., Koh, J.L., Gultekin, S.H., Anderson, J.C., Vogel, H., Sutcliffe, T.L., Jacobs, Y., Steiner, R.D., 2013. Central nervous system stem cell transplantation for children with neuronal ceroid lipofuscinosis. J. Neurosurg. Pediatr 11, 643–652.

Sleat, D.E., Donnelly, R.J., Lackland, H., Liu, C.G., Sohar, I., Pullarkat, R.K., Lobel, P., 1997. Association of mutations in a lysosomal protein with classical late-infantile neuronal ceroid lipofuscinosis. Science 277, 1802–1805.

Sleat, D.E., El-Banna, M., Sohar, I., Kim, K.H., Dobrenis, K., Walkley, S.U., Lobel, P., 2008. Residual levels of tripeptidyl-peptidase I activity dramatically ameliorate disease in late-infantile neuronal ceroid lipofuscinosis. Mol. Genet. Metab. 94, 222–233.

Sleat, D.E., Gin, R.M., Sohar, I., Wisniewski, K., Sklower-Brooks, S., Pullarkat, R.K., Palmer, D.N., Lerner, T.J., Boustany, R.M., Uldall, P., Siakotos, A.N., Donnelly, R.J., Lobel, P., 1999. Mutational analysis of the defective protease in classic late-infantile neuronal ceroid lipofuscinosis, a neurodegenerative lysosomal storage disorder. Am. J. Hum. Genet. 64, 1511–1523.

Sleat, D.E., Wiseman, J.A., El-Banna, M., Kim, K.H., Mao, Q., Price, S., Macauley, S.L., Sidman, R.L., Shen, M.M., Zhao, Q., Passini, M.A., Davidson, B.L., Stewart, G.R., Lobel, P., 2004. A mouse model of classical late-infantile neuronal ceroid lipofuscinosis based on targeted disruption of the CLN2 gene results in a loss of tripeptidyl-peptidase I activity and progressive neurodegeneration. J. Neurosci. 24, 9117–9126.

Sohar, I., Sleat, D.E., Jadot, M., Lobel, P., 1999. Biochemical characterization of a lysosomal protease deficient in classical late infantile neuronal ceroid lipofuscinosis (LINCL) and development of an enzyme-based assay for diagnosis and exclusion of LINCL in human specimens and animal models. J. Neurochem. 73, 700–711.

Sondhi, D., Hackett, N.R., Apblett, R.L., Kaminsky, S.M., Pergolizzi, R.G., Crystal, R.G., 2001. Feasibility of gene therapy for late neuronal ceroid lipofuscinosis. Arch. Neurol. 58, 1793–1798.

Sondhi, D., Hackett, N.R., Peterson, D.A., Stratton, J., Baad, M., Travis, K.M., Wilson, J.M., Crystal, R.G., 2007. Enhanced survival of the LINCL mouse following CLN2 gene transfer using the rh.10 rhesus macaque-derived adeno-associated virus vector. Mol. Ther. 15, 481–491.

Sondhi, D., Peterson, D.A., Edelstein, A.M., del Fierro, K., Hackett, N.R., Crystal, R.G., 2008. Survival advantage of neonatal CNS gene transfer for late infantile neuronal ceroid lipofuscinosis. Exp. Neurol. 213, 18–27.

Viglio, S., Marchi, E., Wisniewski, K., Casado, B., Cetta, G., Iadarola, P., 2001. Diagnosis of late-infantile neuronal ceroid lipofuscinosis: a new sensitive method to assay lysosomal pepstatin-insensitive proteinase activity in human and animal specimens by capillary electrophoresis. Electrophoresis 22, 2343–2350.

Vines, D.J., Warburton, M.J., 1999. Classical late infantile neuronal ceroid lipofuscinosis fibroblasts are deficient in lysosomal tripeptidyl peptidase I. FEBS Lett. 443, 131–135.

Vuillemenot, B.R., Katz, M.L., Coates, J.R., Kennedy, D., Tiger, P., Kanazono, S., Lobel, P., Sohar, I., Xu, S., Cahayag, R., Keve, S., Koren, E., Bunting, S., Tsuruda, L.S., O'Neill, C.A., 2011. Intrathecal tripeptidyl-peptidase 1 reduces lysosomal storage in a canine model of late infantile neuronal ceroid lipofuscinosis. Mol. Genet. Metab. 104, 325–337.

Walus, M., Kida, E., Golabek, A.A., 2010. Functional consequences and rescue potential of pathogenic missense mutations in tripeptidyl peptidase I. Hum. Mutat. 31, 710–721.

Warrier, V., Vieira, M., Mole, S.E., 2013. Genetic basis and phenotypic correlations of the neuronal ceroid lipofusinoses. Biochim. Biophys. Acta 1832, 1827–1830.

Williams, R.E., Mole, S.E., 2012. New nomenclature and classification scheme for the neuronal ceroid lipofuscinoses. Neurology 79, 183–191.

Worgall, S., Sondhi, D., Hackett, N.R., Kosofsky, B., Kekatpure, M.V., Neyzi, N., Dyke, J.P., Ballon, D., Heier, L., Greenwald, B.M., Christos, P., Mazumdar, M., Souweidane, M.M., Kaplitt, M.G., Crystal, R.G., 2008. Treatment of late infantile neuronal ceroid lipofuscinosis by CNS administration of a serotype 2 adeno-associated virus expressing CLN2 cDNA. Hum. Gene Ther. 19, 463–474.

Xu, S., Wang, L., El-Banna, M., Sohar, I., Sleat, D.E., Lobel, P., 2011. Large-volume intrathecal enzyme delivery increases survival of a mouse model of late infantile neuronal ceroid lipofuscinosis. Mol. Ther. 19, 1842–1848.